High-Coherence Electron and Ion Bunches from Laser-Cooled Atoms

2014 J. Phys.: Conf. Ser. 488 012045

(http://iopscience.iop.org/1742-6596/488/1/012045)

Journal of Physics: Conference Series **488** (2014) 012045 doi:10.1088/1742-6596/488/1/012045

High-Coherence Electron and Ion Bunches from Laser-Cooled Atoms

A. J. McCulloch, D. V. Sheludko, C. T. Putkunz, S. D. Saliba, D. J. Thompson, R. W. Speirs, D. Murphy, J. Torrance, B. M. Sparkes, and R. E. Scholten

ARC Centre of Excellence for Coherent X-Ray Science, School of Physics, The University of Melbourne, Australia

E-mail: scholten@unimelb.edu.au

Abstract. Cold atom electron and ion sources produce electron bunches and ion beams by photoionisation of laser cooled atoms. They offer high coherence and the potential for high brightness, with applications including ultrafast electron diffractive imaging of dynamic processes at the nanoscale. Here we present our cold atom electron/ion source, with an electron temperature of less than 10 K and a transverse coherence length of 10 nm. We also discuss experiments investigating space-charge effects with ions and the production of ultra-fast electron bunches using a femto-second laser. In the latter experiment we show that it is possible to produce both cold and fast electron bunches with our source.

1. Introduction

Being able to image the dynamics of atomic-scale processes and produce a "molecular movie" is the ultimate goal of x-ray and electron imaging [1]. This is motivated by a need to understand critical phenomena underlying biology, materials sciences and technological applications. For instance, rational drug design relies on knowing the molecular structure and function of certain membrane proteins [2]. In a bid to achieve this goal many different technologies are being developed. These include billion-dollar x-ray free electron lasers which attempt to produce sufficient brightness in an x-ray beam for single-shot imaging of non-crystalline objects [3].

An alternative to creating very bright x-ray sources is to use electrons, where the sample interaction is 10^4 to 10^6 times stronger [4], far fewer electrons are needed to achieve the same results. The drawback to using electrons, however, is the space-charge effect; that is, the Coulomb interaction within an electron bunch that dramatically reduces the source brightness and coherence. This issue can be overcome if the electron bunch has a uniform ellipsoidal distribution [5].

The ability to shape electron bunches into appropriate ellipsoidal distributions is one of the motivations behind the development of a cold atom electron/ion source (CAEIS) [6]. Other advantages of a CAEIS include the high source coherence due to the low temperatures of the electrons and ions produced from the laser-cooled atoms and the promise of high brightness, with up to 10^6 particles per bunch. Here we present an overview of our CAEIS, some investigation of space-charge effects, and the creation of ultra-fast cold electron bunches.

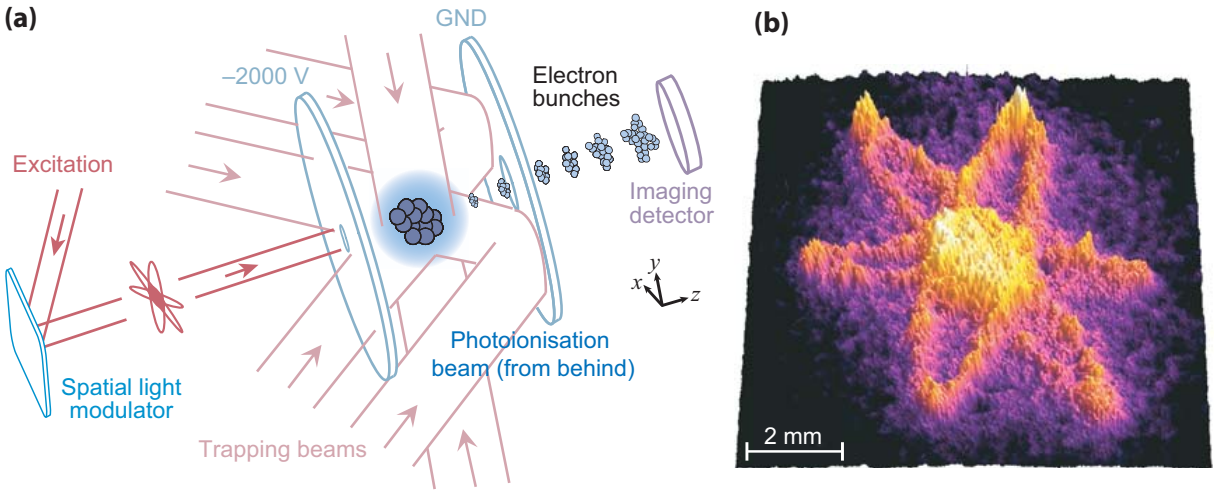

Figure 1. (a) Experimental set-up of the cold atom electron/ion source. (b) False-colour image of electron cloud detected on MCP. From Reference [8].

2. The Cold Atom Electron/Ion Source

2.1. Source of Cold Atoms

In our experiments we laser-cool and trap rubidium-85 atoms. We use an effusive oven to produce hot rubidium, which is then cooled via a Zeeman slower before entering the trapping region. This provides a high-flux source of slow atoms, and is described in more detail in Reference [7]. The atoms are then confined in a magneto-optic trap (MOT) located between two accelerator plates, 55 mm apart. Using this method, up to 10^9 atoms can been trapped with a Gaussian width of less than 1 mm, leading to densities up to 10^{11} cm^{-3}. The atom cloud temperature is approximately 70 μK.

2.2. Creating Shaped Electron and Ion Bunches

To create electron and ion bunches, a two-stage ionisation process is used. Firstly, the trapping and cooling lasers, as well as the magnetic fields of the MOT, are turned off. A pulse of laser light resonant with the D2 $F = 3 \rightarrow F' = 4$ transition (780 nm) is then directed onto the atoms perpendicular the accelerator plates. This pulse is created by placing an acousto-optic modulator in the path of a continuous wave (CW) laser and has a temporal width on the order of microseconds. A 5 ns 480 nm pulsed laser beam is directed onto the excited atoms in a direction parallel to the accelerator plates. The wavelength of the pulsed blue laser can be changed over tens of nanometres to allow for either direct ionisation of the already-excited atoms, or to excite them to a high-lying Rydberg state, where the static accelerator field induces field ionisation.

The pulsed blue laser is focused into a sheet of light at the MOT, with a full-width-half-maximum width of approximately 150 μm. The 780 nm excitation laser profile, meanwhile, is transformed into an arbitrary shape using a spatial-light modulator (SLM). This combination of laser wavelengths and orientations creates the shaped electron and ion bunches, as shown in Fig. 1(a). Approximately 10^5 electrons were produced in each bunch.

2.3. Detection

We select electrons or ions by appropriate choice of polarity for our accelerator front plates (e.g. electrons in Fig. 1a). The electric field strength was approximately 40 kV/m. After constant acceleration, the electrons or ions are propagated for 21.5 cm in a null field, then detected on a microchannel plate detector (MCP) and imaged with a CCD camera to provide 2D spatial

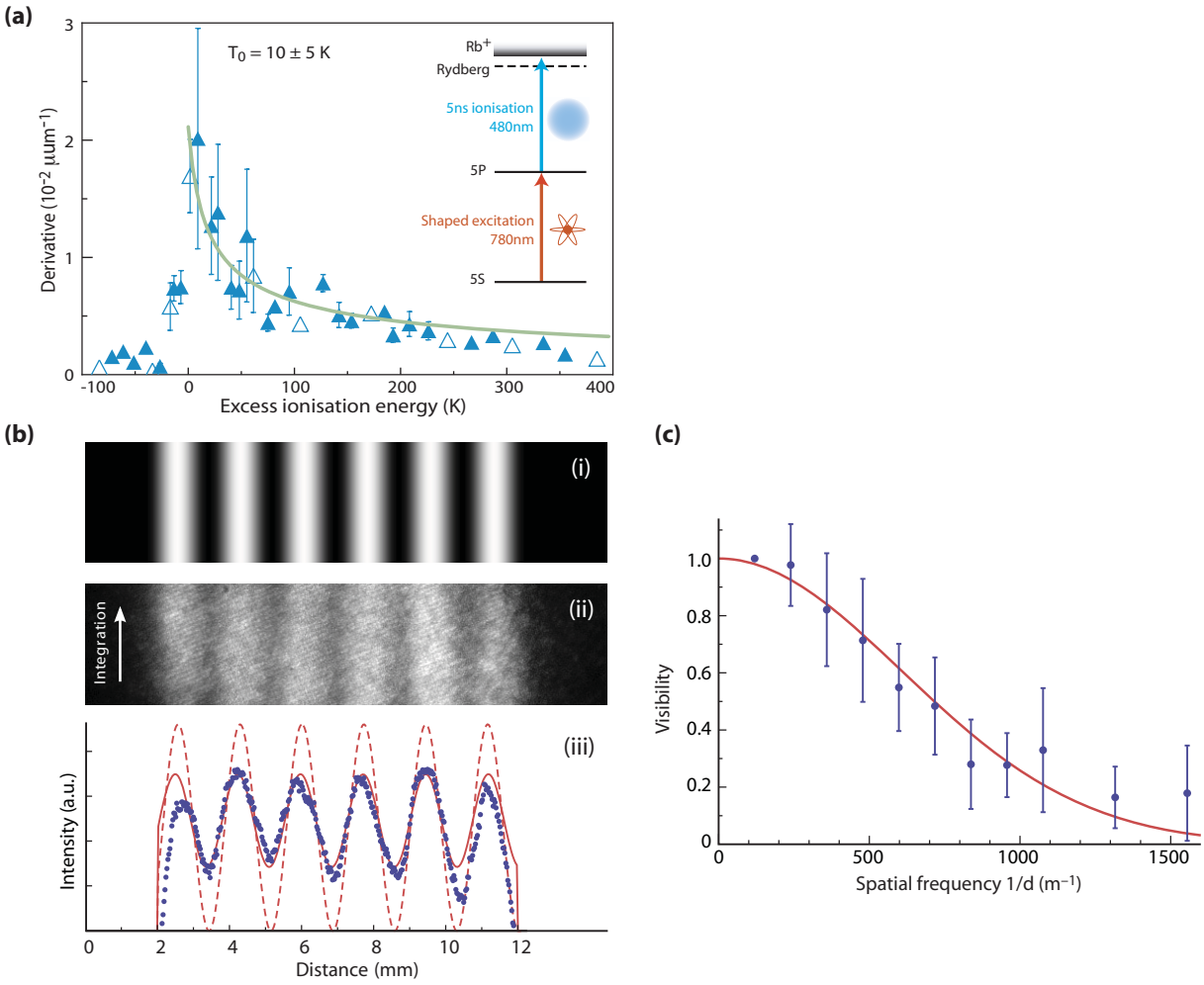

Figure 2. (a) Electron bunch edge width. The error bars indicate one standard deviation over 30 shots, including statistical and systematic uncertainties. An upper limit to source temperature is extracted by fitting Equation 1 to the data (solid line) with excess ionisation energy $\Delta E_c \geq 0$ K. Inset shows the relevant energy levels and transitions in rubidium. From Reference [8]. (b)(i) Desired excitation laser beam intensity profile used to create the SLM phase mask. (ii) Image of resulting shaped electron bunch on MCP. (iii) Integrated line profile of the calculated fully coherent electron distribution (red, dashed), the recorded electron image (blue points), and a fit to the recorded data (red, solid). (c) Visibility of electron bunch pattern as a function of spatial frequency, with a Gaussian fit to the visibility function resulting in $L_c = 7.8 \pm 0.9$ nm. The systematic uncertainty is measuring d was 3%. From Reference [11].

resolution of the bunch, as shown in Fig. 1b). Temporal evolution of the bunch can be determined by monitoring the potential of the grounded component of the MCP.

2.4. Temperature and Coherence Length of Electrons Bunches

The temperature of the electron source can be determined by performing measurements of the divergence of the bunches, which affects the edge acuity. The transverse thermal velocity of the

electron cloud determines the angular spread after propagation via the equation [9]

$$\frac{dQ_e}{dr} = e\kappa \frac{d_1}{2d_1 + d_2}\sqrt{\frac{eF}{d1\,(k_B T_0 + \Delta E)}}, \tag{1}$$

where Q_e is the detector signal proportional to charge, r is the radial coordinate, e is the electron charge, κ is linear magnification, d_1 and d_2 are the distances through which the bunch is accelerated and freely propagated respectively, F is the accelerator field magnitude, k_B is Boltzmann's constant, T_0 is the minimum electron temperature, and ΔE is the excess energy of the electrons after ionisation. By varying the excess energy given to the electrons (by changing the wavelength of the blue laser) and fitting κ and T_0, the minimum temperature of the electrons was found to be $T_0 < 10 \pm 5$ K [8]. The results are shown in Fig. 2(a). The electron temperature is much higher than the cold atom temperature (70 μK) due to intrinsic heating processes encountered during ionisation, such as disorder-induced heating.

From this minimum temperature we can determine the transverse coherence length of the electron bunch via [10]

$$L_c = \hbar/\sqrt{m_e k_B T_0}, \tag{2}$$

where m_e is the mass of the electron. Using the value for T_0 obtained above gives $L_c > 10 \pm 3$ nm. The arbitrary shaping ability of the CAEIS can also be used to directly measure the coherence length. This was achieved by using a sinusoidally shaped excitation laser and measuring the visibility of the electron pattern as a function of spatial frequency (Fig. 2b and 2c), resulting in a measurement of $L_c = 7.8 \pm 0.9$ nm [11]. A coherence length of 10 nm is already sufficient at the source for imaging small biomolecules such as bacteriorhodopsin, where the unit cell length is of order 10 nm. In contrast, photoemission electron sources with electron bunch temperatures of order 10^4 K have an associated coherence length of 0.3 nm.

We have not yet measured the temperature of our ion bunches, but other groups have measured temperatures on the order of milliKelvins, again limited by disorder-induced heating [12].

3. Space-Charge Effects

Space-charge effects within clouds of electrons or ions cause bunch expansion. This is normally an irreversible process and leads to a loss in coherence and brightness. However, if the bunch shape is a uniform ellipsoid then the internal fields are linear, and though the bunch will still expand, the expansion can be reversed by refocusing with conventional linear charged particle optial systems, preserving the initial coherence and brightness of the source. It has been theoretically shown that an initial bunch with a semi-circular transverse distribution and a very narrow longitudinal distribution will evolve into a uniform ellipsoid [5].

Creating such a distribution experimentally is, however, quite challenging. The spatial distribution of the initial bunch depends not only on the excitation beam profile, but also on the initial density of the cold atom cloud, and the time-dependent behaviour of the excitation process. We have simulated these effects using optical Bloch equations, and modelled the evolution of the bunch shape using General Particle Tracer (GPT) simulations [13].

We have investigated space-charge effects using ions rather than electrons because they are far more massive and slower, allowing for longer interaction times. The ion temperature is also orders of magnitude lower than for electrons, so the effects of thermal diffusion are minimal. In combination, the effects of Coulomb interactions within the bunch are much more clearly discernible. Our investigations have led to the discovery of some interesting effects such as the formation of density waves around an initially uniform circular ion bunch. This can be explained by the formation of a diffuse halo of charges around the central core of the bunch. The halo is created by re-absorption of spontaneous emission from the directly excited atoms. The dense

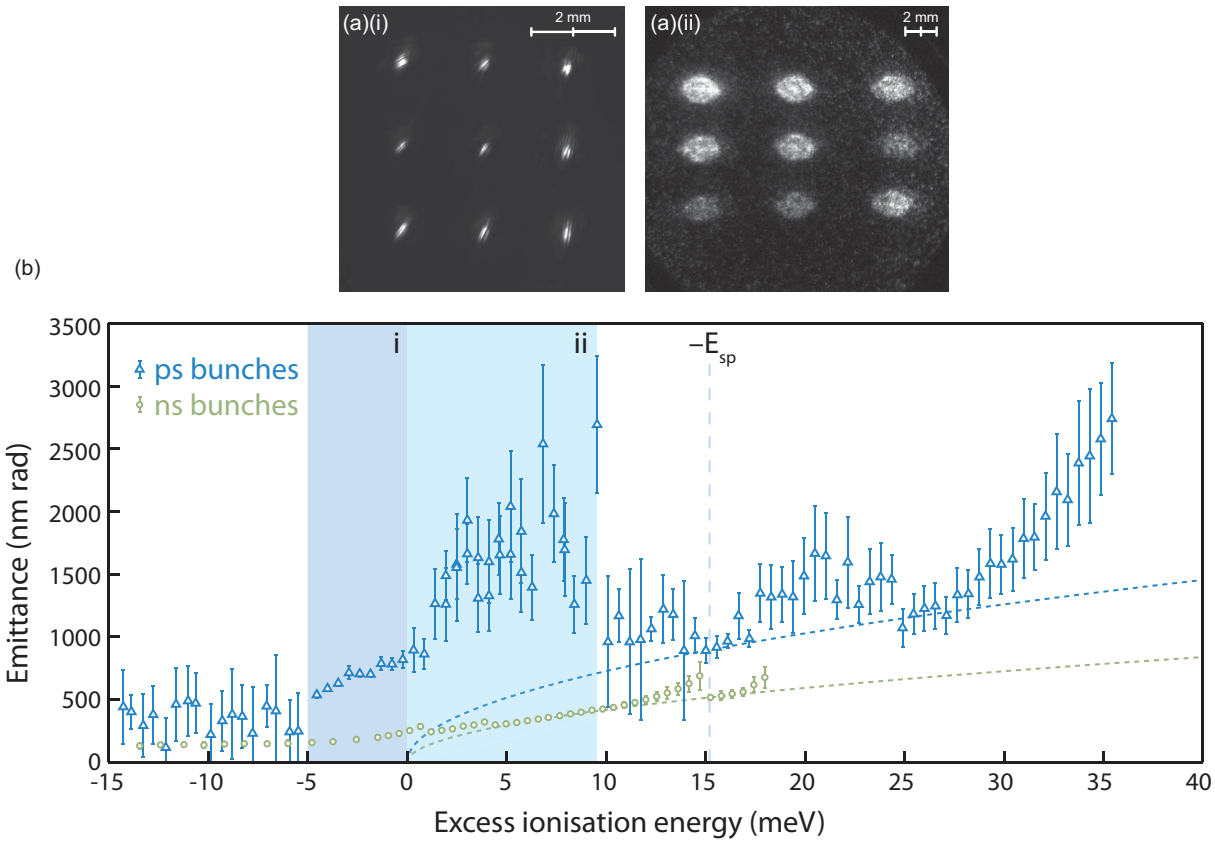

Figure 3. (a) Typical pepperpot images used to extract the emittance of femtosecond-excited CAEIS electron bunches. (i) A CCD image of the laser pulse used to excite the atoms. (ii) Detected electron signal on MCP for an ionisation wavelength of 478.00 nm. (b) Measured radial emittance as a function of excess ionisation energy. Each point represents 50 single-shot measurements with the error bars indicating one standard deviation combined from the statistical deviation and systematic uncertainties. The dashed lines are theoretical plots. For more information see Reference [16].

core then expands into the halo, due to space-charge repulsion, and creates a high-density ring. We have also investigated the space-charge interaction of parallel beamlets to see the influence of overlapping self-fields [14]. Our studies show good agreement between simulations and experiments. The simulations reveal the sensitivity of the visibility of the high-density features to the initial ion temperature: the structure is lost at temperatures of a few tens of Kelvin, highlighting the advantages of the cold atom source in comparison with conventional sources, which operate at room temperature or above, for studying these effects.

4. Ultra-Fast Cold Electrons

Ultra-fast electron diffraction enables the study of molecular structural dynamics with high resolution at sub-picosecond timescales. This is important for understanding biochemical dynamics such as protein folding and regulation, as well as the formation of cracks in novel materials [4, 15]. Ultrafast exposure times will also allow high intensity imaging of radiation sensitive samples, such as biologically relevant molecules, to obtain sufficient information about the molecule before it dissociates, known as “diffract-before-destroy” imaging.

To achieve this with our CAEIS, we replaced the CW 780 nm excitation laser switched via

an acousto-optic modulator with a femto-second laser. With femtosecond excitation, the initial electron pulse duration is limited by the spatial and temporal extent of the overlap between the new femtosecond pulses and the 5 ns pulses of 480 nm light. The overlap produces a shaped pulse of electrons or ions with a minimum duration of 150 ps [16].

The high bandwidth inherent to short laser pulses might be expected to increase the excess energy spread of the electrons and thus destroy their transverse coherence. We performed an emittance measurement using the pepperpot method. Instead of using a physical pepperpot, we shaped the femto-second excitation as shown in Fig. 3(a)(i) and measured the spatial distribution of the electron bunches at the MCP detector. By knowing the initial and final electron beamlet distributions, the emittance ε_r can be calculated (for more details see Reference [16]). The pepperpot measurements were performed for a series of different blue laser wavelengths, similar to the temperature measurements discussed in Section 2, and compared to results with CW excitation.

From the results (Fig. 3b) it can be seen that in Region (i) – i.e. just below the field-free ionisation threshold – the emittance increases, coinciding with an increase in ionisation efficiency. In this region the electron bunches that are produced are both ultrafast, and still highly coherent. In Region (i) the blue laser couples the $5P_{3/2}$ state to one or more field-ionising Rydberg states, resulting in an electron bunch with minimal spread. Above threshold, in Region (ii), the emittance increases dramatically due to the opening of an alternative ionisation pathway: when the energy of the ionisation laser is above threshold, the blue laser couples the $5P_{3/2}$ state directly to the continuum. In this case the large near-resonant bandwidth of the 780 nm femtosecond pulse substantially increases the energy spread. As the excess ionisation energy increases further, a decrease in emittance is observed. This shows that the bandwidth of the femtosecond laser is not contributing appreciably to the energy spread.

Below Region (i) the emittance is approximately constant ($\varepsilon_r = 538 \pm 26$ nm), limited by heating during the extraction process. In the same region, the emittance from the CW excitation laser was 141 ± 7 nm. Though the femtosecond emittance is larger, the corresponding coherence length is still relatively large for an electron source, at $L_c = 4.0 \pm 0.2$ nm [16].

5. Conclusion

We have presented our cold atom electron/ion source, including characterisation of the electron temperature and coherence length. We have investigated the effect of space-charge on ion bunches, including the formation of density waves due to spontaneous emission and reabsorption from the main interaction region. Finally we presented results showing that we can produce ultra-fast (150 ps) electron clouds, while maintaining an coherence length of 4 nm. To improve the emittance further we are looking to reduce the temperature by using Rydberg blockade to overcome disorder-induced heating effects, and using our shaping ability to overcome space-charge effects.

References

[1] Chapman H N, Hebeisen C T, Ernstorfer R, Harb M, Deyirmenjian V B, Jordan R E, and Dwayne Miller RJ 2006 *Phil. Trans. Royal. Soc.* A **364** 741
[2] Pinto L H, Holsinger L J, and Lamb R A 1992 *Cell* **69** 517
[3] Chapman H N, Fromme P, Barty A, White T A, *et al.* 2011 *Nature* **470** 73
[4] Sciaini G, and Miller R J D 2011 *Rep. Prog. Phys.* **74** 096101
[5] Luiten O J, van der Geer S B, de Loos M J, Kiewiet F B, and van der Wiel M J 2004 *Phys. Rev. Lett.* **93** 094802
[6] Claessens B J, van der Geer S B, Taban G, Vredenbregt E J D, and Luiten O J 2005 *Phys. Rev. Lett.* **95** 164801
[7] Bell S C, Junker M, Jasperse M, Turner L D, Lin Y-J, Spielman I B, and Scholten R E 2010 *Rev. Sci. Instrum.* **81** 013105

[8] McCulloch, A J, Sheludko D V, Saliba S D, Bell, S C, Junker M, Nugent K A, and Scholten R E 2011 *Nature Phys.* **7** 785
[9] Sheludko D V PhD Thesis, The University of Melbourne 2010. http://repository.unimelb.edu.au/10187/9228
[10] van Oudheusden T *et al.* 2007 *J. Appl. Phys.* **102** 093501
[11] Saliba S D, Putkunz C T, Sheludko D V, McCulloch A J, Nugent K A, and Scholten R E 2012 *Opt. Exp.* **20** 3967
[12] Bannasch G, Killian T C, and Pohl T 2013 *Phys. Rev. Lett.* **110** 253003
[13] http://www.pulsar.nl/gpt
[14] Murphy D *et al.*, In progress
[15] Schotte F *et al.* 2003 *Science* **300** 1944
[16] McCulloch A J, Sheludko D V, Junker M, and Sholten R E, 2013 *Nature Commun.* **4** 1692